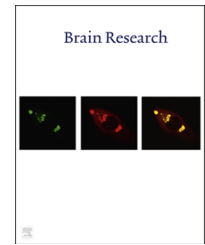


Available online at www.sciencedirect.com
www.elsevier.com/locate/brainres

Research Report

Role for electrical synapses in shaping the output of coupled peptidergic neurons from *Lymnaea*



Christopher C. Beekharry, Guan Z. Zhu, Neil S. Magoski*

Department of Biomedical and Molecular Sciences, Queen's University, Kingston, ON, Canada K7L 3N6

ARTICLE INFO

Article history:

Accepted 20 January 2015

Available online 30 January 2015

Keywords:

Gap junction

Fenamate

Tonic firing

Lymnaea stagnalis

Mollusc

ABSTRACT

Electrically coupled neurons communicate through channel assemblies called gap junctions, which mediate the transfer of current from one cell to another. Electrical synapses ensure spike synchronization and reliable transmission, which influences bursting patterns and firing frequency. The present study concerns an electrically coupled two-neuron network in the gastropod mollusc, *Lymnaea stagnalis*. The neurons, designated Visceral Dorsal 1 (VD₁) and Right Parietal Dorsal 2 (RPD₂), are peptidergic, innervate aspects of the cardio-respiratory system, and show strong coupling, such that they fire synchronously. Using dual sharp-electrode current-clamp recording and morphological staining in isolated brain preparations, the hypothesis that the electrical synapse is necessary for accurate network output was tested. We found that both cells make extensive projections within and out of the brain, including across the visceral–parietal connective, which links VD₁ and RPD₂. Cutting this connective uncoupled the neurons and disrupted the firing rate and pattern of RPD₂ more than VD₁, consistent with VD₁ being the master and RPD₂ the follower. The electrical synapse was inhibited by select gap junction blockers, with niflumic acid and 5-nitro-2-(3-phenylpropylamino) benzoic acid decreasing the VD₁→RPD₂ and RPD₂→VD₁ coupling coefficients, whereas carbenoxolone, α -glycyrrhetic acid, meclofenamic acid, and quinine were ineffective. There was little-to-no impact on VD₁↔RPD₂ firing synchrony or frequency when coupling was reduced pharmacologically. However, in the presence of gap junction blockers, suppressing the activity of VD₁ by prolonged hyperpolarization revealed a distinct, low-frequency firing pattern in RPD₂. This suggests that strong electrical coupling is key to maintaining a synchronous output and proper firing rate.

© 2015 Elsevier B.V. All rights reserved.

Abbreviations: A, anal nerve; CC, cerebral commissure; CNS, central nervous system; CP, cutaneous pallial nerve; DMSO, dimethyl sulfoxide; G, genital nerve; HEPES, N-2-hydroxyethylpiperazine-N'-2-ethanesulphonic acid; I, intestinal nerve; NFA, niflumic acid; NPPB, 5-nitro-2-(3-phenylpropylamino) benzoic acid; RIP, right internal parietal nerve; REP, right external parietal nerve; RPD₂, neuron Right Parietal Dorsal 2; VD₁, neuron Visceral Dorsal 1

*Correspondence to: Queen's University, Department of Biomedical and Molecular Sciences, 4th Floor, Botterell Hall, 18 Stuart Street, Kingston, ON, Canada K7L 3N6. Fax: +1 613 533 6880.

E-mail address: magoski@queensu.ca (N.S. Magoski).

<http://dx.doi.org/10.1016/j.brainres.2015.01.039>

0006-8993/© 2015 Elsevier B.V. All rights reserved.

1. Introduction

Gap junction channels form the basis of the electrical synapse by linking the intracellular compartment of one neuron to another, and allowing the transfer of electrical current or small molecules (Bennett, 2000; Bennett and Zukin, 2004; Söhl et al., 2005). Electrical coupling promotes the synchronization of spiking or rapid transmission of action potentials within circuits requiring short latency responses, particularly those mediating escape or sensory processing (Furshpan and Potter, 1959; Diamond and Huxley, 1968; Galarreta and Hestrin, 1999; Landisman et al., 2002). Furthermore, groups of neurons, from both vertebrates and invertebrates, generate distinct rhythmic output of action potentials due, in part, to electrical coupling (Gähwiler et al., 1978; Blankenship and Haskins, 1979; Haskins and Blankenship, 1979; Getting, 1989; Norekian, 1999; Traub et al., 2001; Long et al., 2005; Apostolides and Trussell, 2014). Models of coupled oscillatory systems indicate that electrical coupling can either increase or decrease the frequency of an oscillator, depending on the membrane potential of the coupled neuron or the strength of the coupling, which provides a flexible mechanism for modifying the output of the neural network (Kepler et al., 1990; Ypey et al., 1980; Ermentrout, 1985; Horn et al., 2012).

The present study concerns a two-neuron system from the central nervous system (CNS) of the gastropod pulmonate mollusc, *Lymnaea stagnalis* (the great pond snail). The identified neurons in question are known as Visceral Dorsal 1 (VD₁) and Right Parietal Dorsal 2 (RPD₂), and they are connected by a strong electrical synapse (Benjamin and Winlow, 1981; Benjamin and Pilkington, 1986; Wildering et al., 1991a,b; Wildering and Janse, 1992). The VD₁/RPD₂ system was shown by prior studies to most prominently innervate the heart, mantle, and pneumostome, suggesting the neurons have a role in cardio-respiratory control (Kerkhoven et al., 1991; Ewadinger et al., 1996). Moreover, as animals age, there is an increased mortality associated with reduced VD₁↔RPD₂ coupling (Wildering et al., 1991b). The two neurons are considered a system because they both express the same assortment of peptides (Bogerd et al., 1991; Kerkhoven et al., 1992; Ewadinger et al., 1996) and function electrophysiologically in unison, as the robust coupling guarantees synchronous firing.

Here, we focus on how the disruption of electrical coupling influences the synchrony and firing of the VD₁/RPD₂ system. When the electrical synapse was abolished, through axotomy of the commissure that connects the neurons, it caused complete desynchronization of the network. In addition, attenuating coupling with select gap junction blockers could lead to changes in spike frequency when the drive to fire was removed by hyperpolarizing VD₁. Thus, electrical synapses are required for synchronous network output and the proper patterning of firing. This may be important for appropriate cardio-respiratory function and promoting animal survival.

2. Results

2.1. Neurons VD₁ and RPD₂ send axonal projections throughout the brain and to the periphery

Following dissection of the CNS, the cerebral commissure was cut and the brain pinned down flat with the dorsal surface up. In this position, neurons VD₁ and RPD₂ could be seen within the visceral and right parietal ganglion, respectively. They are usually larger than the surrounding cells and can be identified by their whiter color in comparison to other neurons. Although there are prior reports of VD₁ and RPD₂ morphology (Soffe and Benjamin, 1980; Benjamin and Pilkington, 1986; Kerkhoven et al., 1991), they were either focused on a specific projection or carried out with animals from suppliers. Our *Lymnaea* are laboratory-reared; thus, to look for potential differences in morphology between these populations, Lucifer yellow was ionophoretically injected into VD₁ and/or RPD₂ with constant hyperpolarizing current for 30 min (see Section 4 for details). In a few preparations ($n=3$), both VD₁ and RPD₂ were stained with Lucifer yellow. VD₁ was normally found in the center lower portion of the visceral ganglion, while RPD₂ was located at the lowest left portion of the right parietal ganglion (Fig. 1A). Both cells sent axons out through various nerves originating from the left parietal, visceral, and right parietal ganglia, as well as to other parts of the CNS.

For the majority of preparations, only VD₁ or RPD₂ were filled with Lucifer yellow. Ewadinger et al. (1994) demonstrated that, despite strong VD₁↔RPD₂ electrical coupling, Lucifer yellow delivered into one of these neurons does not dye-couple to its partner. Thus, our fills likely represent the morphology of just the injected neuron. Staining of VD₁ ($n=13$) typically revealed axons projecting through the cutaneous pallial, intestinal, and genital nerves from the visceral ganglion, as well as the internal and external nerves from the right parietal ganglion (Fig. 1B and C). Axons were observed ~80% of the time in the cutaneous pallial and right internal parietal nerves, and to a lesser extent in the left parietal, intestinal, genital, and right external parietal nerves (see Table 1 for percent of preparations with an axon in a given nerve). VD₁ also sent projections through the right and left parietal ganglia, then the left and right pleural ganglia, into one or both cerebral ganglia, and through the cerebral commissure (Fig. 1D). For RPD₂ ($n=19$), the extent of the projections was less, and restricted to nerves originating from the visceral and two parietal ganglia (Fig. 1E and F). In ~60% of preparations; RPD₂ axons passed through the anal and intestinal nerves, with relatively fewer cases of projections through the left parietal, genital, or right internal and external parietal nerves (Table 1). Note that in all fills, both VD₁ and RPD₂ always sent a large axon across the visceral-right parietal commissure. However, that aside, none of our preparations showed any additional invariant projections, with no particular nerves always having an axon present.

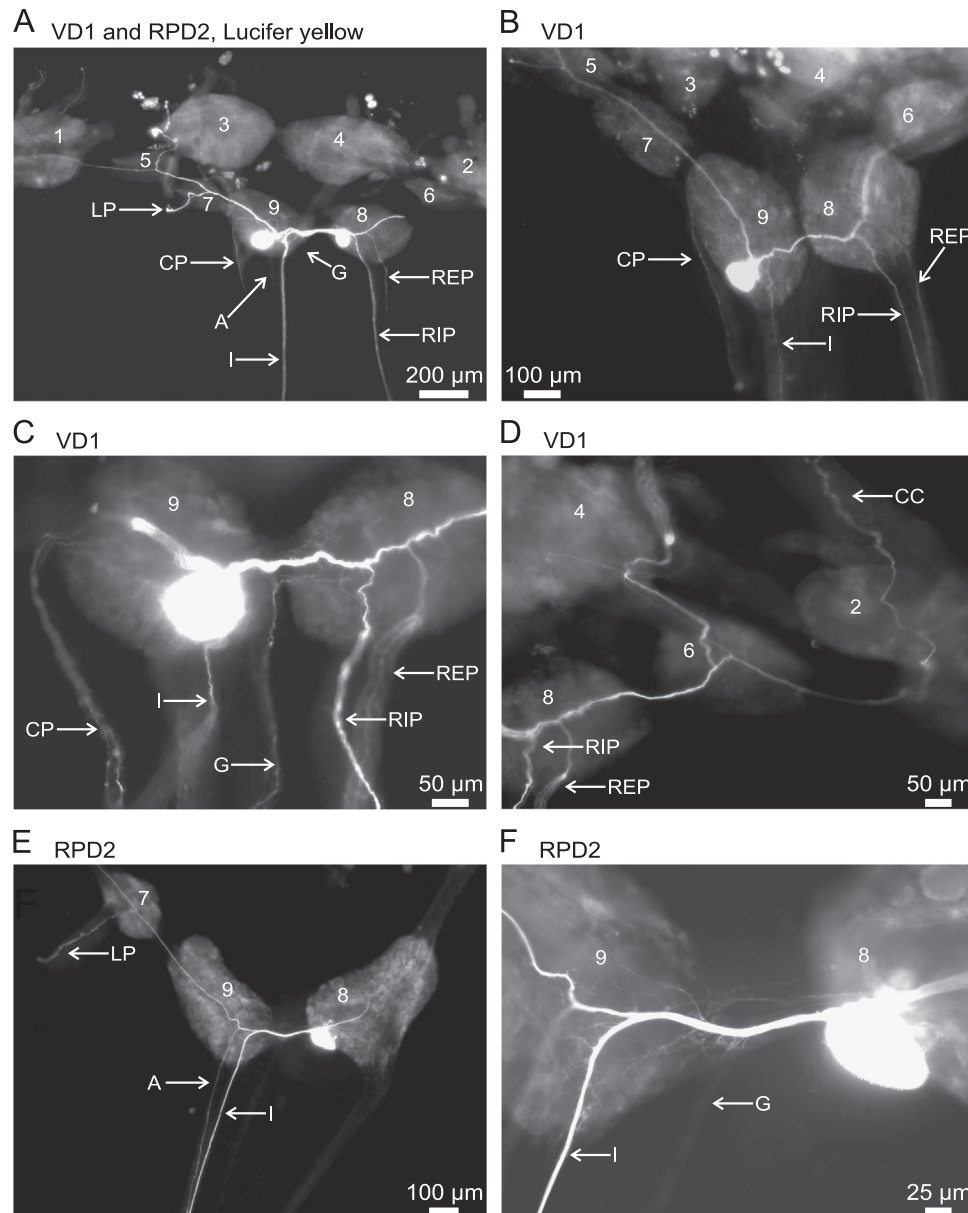


Fig. 1 – The morphology of neurons VD_1 and RPD_2 . (A) Intracellular staining with Lucifer yellow ionophoretically injected into VD_1 and RPD_2 . The CNS is shown dorsal surface up and essentially flat, with the cerebral commissure cut and the cerebral ganglia laid out ventral surface up. Dual fill of VD_1 and RPD_2 reveals axon projections (from one or both neurons) in the left parietal (LP), cutaneous pallial (CP), anal (A), intestinal (I), genital (G), right internal parietal (RIP), and right external parietal (REP) nerves (denoted by white arrows). Ganglia are numbered as per the convention of [Syed and Winlow \(1991\)](#): left and right cerebral ganglia (1, 2), left and right pedal ganglia (3, 4), left and right pleural ganglia (5, 6), left and right parietal ganglia (7,8), and visceral (9) ganglion; the buccal ganglia are not shown. (B, C) Single intracellular dye fills of VD_1 . Panel B shows a stained axon within the left parietal nerve with a projection through to the left pleural ganglion, as well as axons in the cutaneous pallial and anal nerves plus a projection across the visceral-right parietal commissure and through the right internal and external parietal nerves. Panel C is a higher magnification of a different VD_1 , with the same projections as panel B, along with an axon in the genital nerve. (D) Dye injection of another VD_1 also reveals an axon projecting through to the right pleural and cerebral ganglia, with the latter going through the cerebral commissure (CC). (E, F) Single intracellular dye fills of RPD_2 . Projections from RPD_2 can be seen in panel E traveling through the visceral-right parietal commissure to the visceral and left parietal ganglia, before branching off into the anal, intestinal, and left parietal nerves. At greater magnification in panel F, another RPD_2 sends a main axon to the visceral ganglion, which then branches through the intestinal and genital nerves.

Table 1 – Axonal projections of VD₁ and RPD₂.

Nerve	Innervation	Presence of axon in nerve (%)	
		VD ₁ (n=13)	RPD ₂ (n=19)
Left parietal (LP)	Mantle edge	62	47
Cutaneous pallial (CP)	Posterior mantle	77	37
Anal (A)	Pneumostome	15	63
Intestinal (I)	Gonad, vagina, gut, pericardium	31	63
Genital (G)	Prostate, receptaculum seminis	62	42
Right internal parietal (RIP)	Mantle, pneumostome, osphradium	85	32
Right external parietal (REP)	Mantle near pneumostome	62	32

Areas of innervation are based on [Janse \(1974\)](#). See [Fig. 1](#) for the location of nerves in the *Lymnaea* CNS. Data represent single neurons stained with Lucifer yellow.

2.2. VD₁ and RPD₂ are strongly coupled

In the isolated CNS, a strong, reciprocal electrical synapse between VD₁ and RPD₂ was seen under dual, sharp-electrode current-clamp. In normal *Lymnaea* saline (see [Section 4](#) for details) injecting 0.5 nA of negative current into either VD₁ or RPD₂ hyperpolarized both the neuron receiving the current, as well as the coupled partner, for the duration of the injection ([Fig. 2A](#)). The strength of electrical coupling was assayed by calculating the coupling coefficient in both directions (VD₁→RPD₂ and RPD₂→VD₁) by dividing the peak hyperpolarization (ΔV_m) of the uninjected neuron by that of the injected neuron. During hyperpolarizing current injection, the membrane potential did not always reach a steady-state; rather, it sometimes peaked and began to recover or “sag” back to baseline, which has been reported previously for the VD₁↔RPD₂ synapse ([Ewadinger et al., 1996](#)). In those cases, the ΔV_m was taken from the peak of the sag to the baseline membrane potential. The coupling coefficient was large in both directions, as much of the hyperpolarization evoked in the injected neuron transferred to the uninjected cell. Moreover, coupling was asymmetrical, with the VD₁→RPD₂ synapse (n=40) presenting a coefficient of ~0.7, which was significantly different from the ~0.5 coefficient of the reciprocal RPD₂→VD₁ synapse (n=34) ([Fig. 2B](#)). Furthermore, the input resistance of the two neurons was significantly different, with VD₁ (n=41) being greater at ~100 M Ω , compared to RPD₂ (n=35) at ~50 M Ω ([Fig. 2C](#)). Note, the sag in voltage during hyperpolarization was largely eliminated by an extracellular saline containing high concentrations of divalent cations (24.6 mM Ca²⁺ and 9 mM Mg²⁺) (n=4). If the sag was the result of activating inwardly rectifying K⁺ channels, the effect of the high-divalent saline may be due to divalent metal block of the inward rectifier ([Yamashita et al., 1994](#); [Jow and Numann, 1998](#)).

2.3. Cutting the commissure between the visceral and right parietal ganglia decouples VD₁ and RPD₂

In control preparations (n=8), VD₁ and RPD₂ fired tonically at 0.94±0.06 Hz and in near absolute synchrony ([Fig. 3 A, left](#)). Accordingly, cross-correlation analysis of these pairs ([Fig. 3B, right](#)) provided an average peak cross-correlation estimate of 0.97±0.01 (n=8), with 1.0 representing complete correlation. To see how removal of electrical coupling affected the output

of the two neurons, the commissure between the visceral and right parietal ganglion (which always contained axons from both neurons) was cut. This resulted in decoupling of the VD₁/RPD₂ network, and RPD₂ no longer fired in synchrony with VD₁ (n=8) ([Fig. 3B](#)), which is consistent with [Wildering et al. \(1991a\)](#), who indicated that VD₁ was the leader and drives the output of the network. In axotomized preparations, the RPD₂ (n=4) firing frequency slowed dramatically to 0.12±0.04 Hz, which was significantly different from the control rate ($F_{2,17}=48.9$, $p<0.0001$, one-way ANOVA; $p<0.01$, Dunnett multiple comparisons test). The activity of VD₁ (n=8) following axotomy was also reduced, albeit to the lesser degree of 0.69±0.07 Hz, which was significantly different from control ($F_{2,17}=48.9$, $p<0.0001$, one-way ANOVA; $p<0.01$, Dunnett multiple comparisons test). This drop in VD₁ firing rate could have been due to other, inhibitory interneurons becoming more active or more potent in the absence of an intact commissure. However, when a separate set of axotomized VD₁ neurons was examined in high divalent saline (24.6 mM Ca²⁺ and 9 mM Mg²⁺), to reduce polysynaptic chemical input ([Berry and Pentreath, 1976](#)), the frequency remained below control, at 0.52±0.08 Hz (n=4), and was not different from axotomized VD₁ in normal saline ($p>0.05$, Student's paired t-test). To ensure that coupling was completely lost, negative current injection into either VD₁ or RPD₂ failed to elicit any hyperpolarizing response in the corresponding neuron ([Fig. 3C](#)).

2.4. NFA or NPPB attenuate VD₁↔RPD₂ coupling

If physical disruption of the region presumed to be the location of the gap junction decoupled the VD₁/RPD₂ network, pharmacological inhibition of the electrical synapse may have similar effects. To explore this, the isolated brain preparation was exposed for 5 min to one of various gap junction blockers, including carbenoxolone, α -glycyrrhetic acid, meclofenamic acid, niflumic acid (NFA), 5-nitro-2-(3-phenylpropylamino) benzoic acid (NPPB), and quinine ([Davidson and Baumgarten, 1988](#); [Harks et al., 2001](#); [Srinivas et al., 2001](#); [Srinivas and Spray, 2003](#)). We previously found that some of these reagents blocked junctional communication between bag cell neurons from the marine gastropod mollusc, *Aplysia californica*. Thus, NFA, NPPB, and meclofenamic acid were applied at concentrations that inhibit both *Aplysia* ([Dargaie et al., 2014](#)) and other gap junctions ([Harks et al., 2001](#); [Srinivas and Spray, 2003](#)). While α -glycyrrhetic

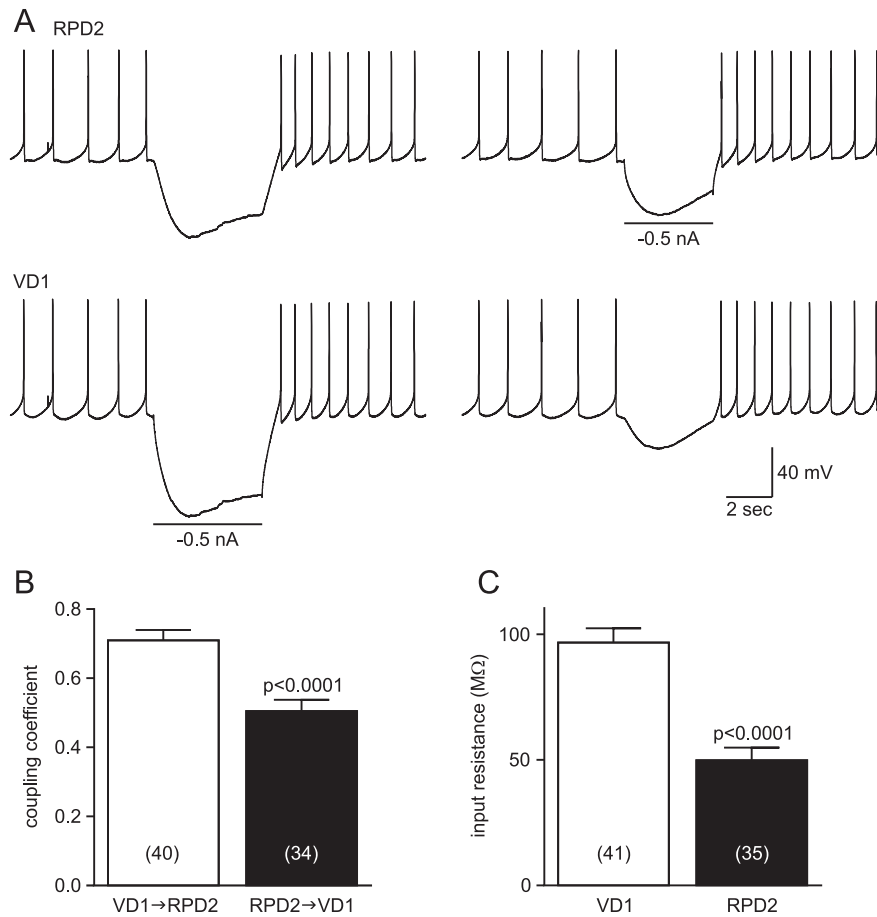


Fig. 2 – VD_1 and RPD_2 are strongly coupled. (A) Dual, sharp-electrode current-clamp from VD_1 and RPD_2 in normal *Lymnaea* extracellular saline using electrodes filled with 0.5 M KCl. Neurons are strongly electrically coupled and fire synchronously. Negative current of 0.5 nA from the amplifier is injected into either VD_1 (left) or RPD_2 (right) as indicated by the length of the bar, hyperpolarizing one cell silences the other neuron, and vice versa. Both neurons showed sagging of the hyperpolarization during current injection. Scale bars apply to all traces. **(B)** Summary data comparing the strength of $VD_1 \leftrightarrow RPD_2$ electrical coupling. Couple coefficients are calculated from the hyperpolarization in membrane potential of the uninjected cell divided by that of the injected cell. Although both coupling coefficients are high, the $VD_1 \rightarrow RPD_2$ coupling is significantly stronger (Student's unpaired t-test). The number of trials is shown within the bars, and represents the numbers of pairs. In most cases, these are from the same animal. **(C)** Average input resistance data from VD_1 and RPD_2 calculated from the peak decrease in membrane potential divided by the current (0.5 nA) injected into the cell. The average input resistance of VD_1 is significantly greater than that of RPD_2 (Student's unpaired t-test). The number of trials is shown within the bars, and represents the number of single cells.

acid, carbenoxolone, and quinine, which were ineffective in *Aplysia*, were employed at levels equal to or greater than those used by others on various preparations (Davidson and Baumgarten, 1988; Srinivas et al., 2001; Cruikshank et al., 2004; Ermentrout et al., 2004; Cao and Nitabach, 2008).

Upon hyperpolarizing VD_1 in the presence of 100 μ M NFA ($n=11$), the strength of the $VD_1 \rightarrow RPD_2$ synapse was clearly decreased, as seen by a reduction in coupling coefficient (Fig. 4A). The effect was similar for 200 μ M NFA ($n=5$), and the differences in coupling coefficient were significant for both concentrations (Fig. 4B, left and middle pairs of bars). Coupling from $RPD_2 \rightarrow VD_1$, although weaker than $VD_1 \rightarrow RPD_2$, was also decreased by 100 μ M NFA ($n=11$) and to an extent that the difference was significant (Fig. 4B, right pairs of bars). Nevertheless, the decrease in coupling was not enough to eliminate the synchronous output of the network. In 100 μ M NFA ($n=11$),

VD_1 and RPD_2 continued to fire together, with the frequency of spiking before (0.79 ± 0.05 Hz) being not significantly different from that after (0.69 ± 0.05 Hz) NFA addition ($p > 0.05$, Student's paired t-test). With respect to input resistance, no significant changes were observed in either neuron after drug application (Fig. 4C). That stated, this particular data set showed some variability in input resistance for both neurons. This likely arose from input resistance being mainly dependent on the change in voltage to the -0.5 nA step, which could fluctuate between preparations. Conversely, because coupling coefficient was derived from the ratio of the two hyperpolarizations following the same -0.5 nA pulse, it tended to be more consistent, which is in keeping with prior reports indicating that junctional conductance is relatively invariant (Wildering et al., 1991b).

The effect of NPPB was similar to NFA. Following negative current injection into VD_1 , the coupling was noticeably depressed

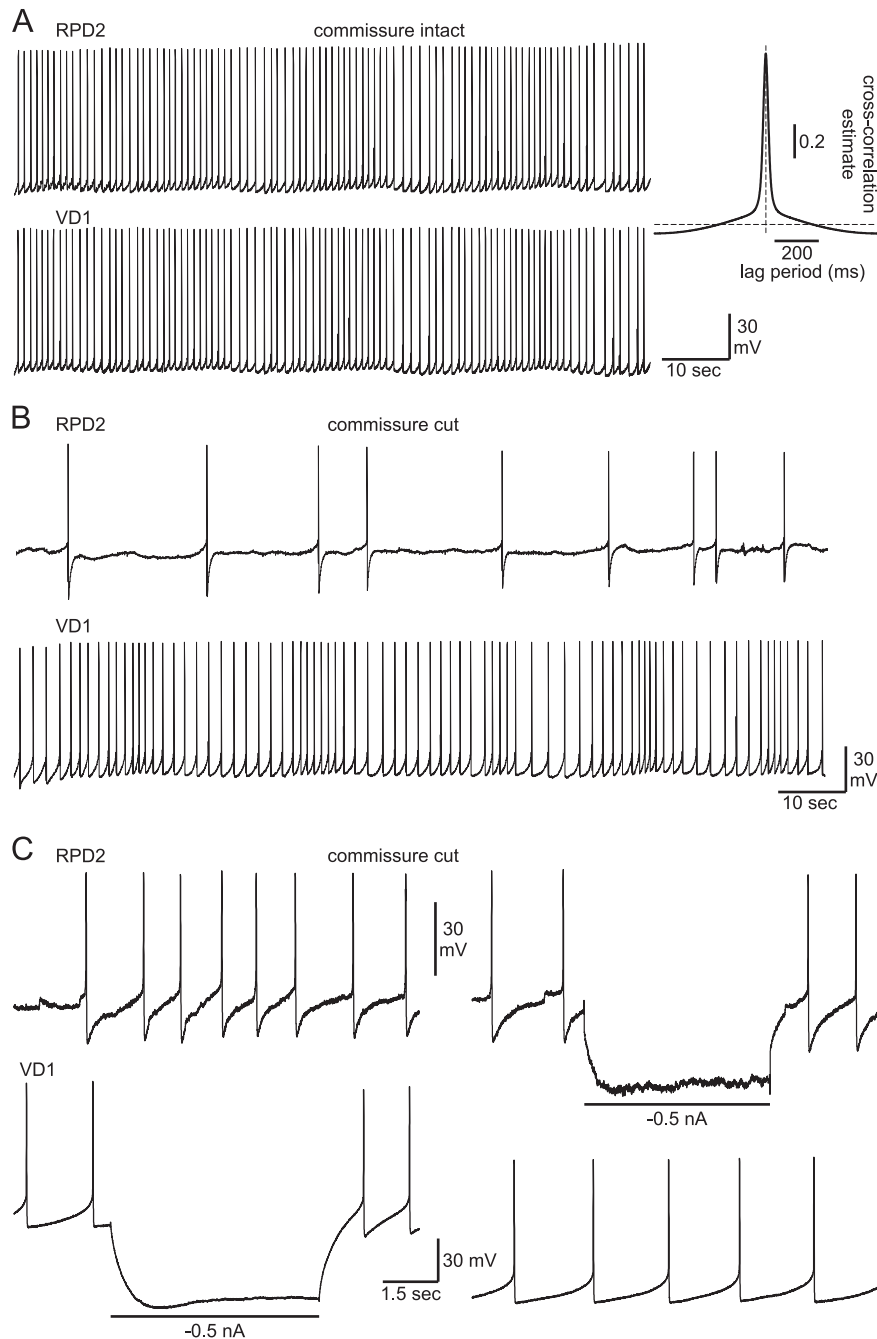


Fig. 3 – Cutting the visceral–right parietal commissure decouples VD₁ and RPD₂. Membrane potential recording of VD₁ and RPD₂ with the visceral–right parietal commissure intact (*left*). The neurons fire tonically and in synchrony at ~1 Hz. Scale bars apply to both traces. Cross-correlogram of the neurons indicating the degree to which the VD₁ and RPD₂ voltage traces match (*right*). Intersecting dashed lines at zero denotes perfect correlation. The strong spike timing correlation between these two neurons yields a cross-correlation estimate of essentially 1, very near the intersection. (A) In different preparations, cutting the commissure (the presumed location of the gap junctions and/or the axons leading to the gap junctions), lowers the activity of VD₁ to some extent (~0.6 Hz), while the spiking of RPD₂ slows markedly (~0.1 Hz) and is no longer in phase with VD₁. Scale bars apply to both traces. (B) Following cutting of the commissure, negative current injection of 0.5 nA into either VD₁ (*bottom-left*) or RPD₂ (*top-right*), fails to hyperpolarize the corresponding neuron. Time base applies to both sets of traces.

in 100 μ M NPPB (Fig. 5A). On average, the coupling coefficient of both the VD₁→RPD₂ ($n=10$) and the RPD₂→VD₁ ($n=10$) synapse decreased by over half, a difference that was significant (Fig. 5B). As with NFA, the input resistance did not change significantly after the application of NPPB (Fig. 5C). Similarly, NPPB did not decouple the VD₁/RPD₂ network, and the output from both cells

was largely unaffected. Compared to the firing frequency before 100 μ M NPPB ($n=10$) (0.94 ± 0.05 Hz), the neurons continued to fire in synchrony after introducing the drug (0.95 ± 0.14 Hz) ($p > 0.05$, Student's paired t -test). Even though NFA and NPPB were able to lower coupling within the VD₁/RPD₂ network, the other blockers, 50 μ M α -glycyrrhetic acid ($n=4$), 100 μ M

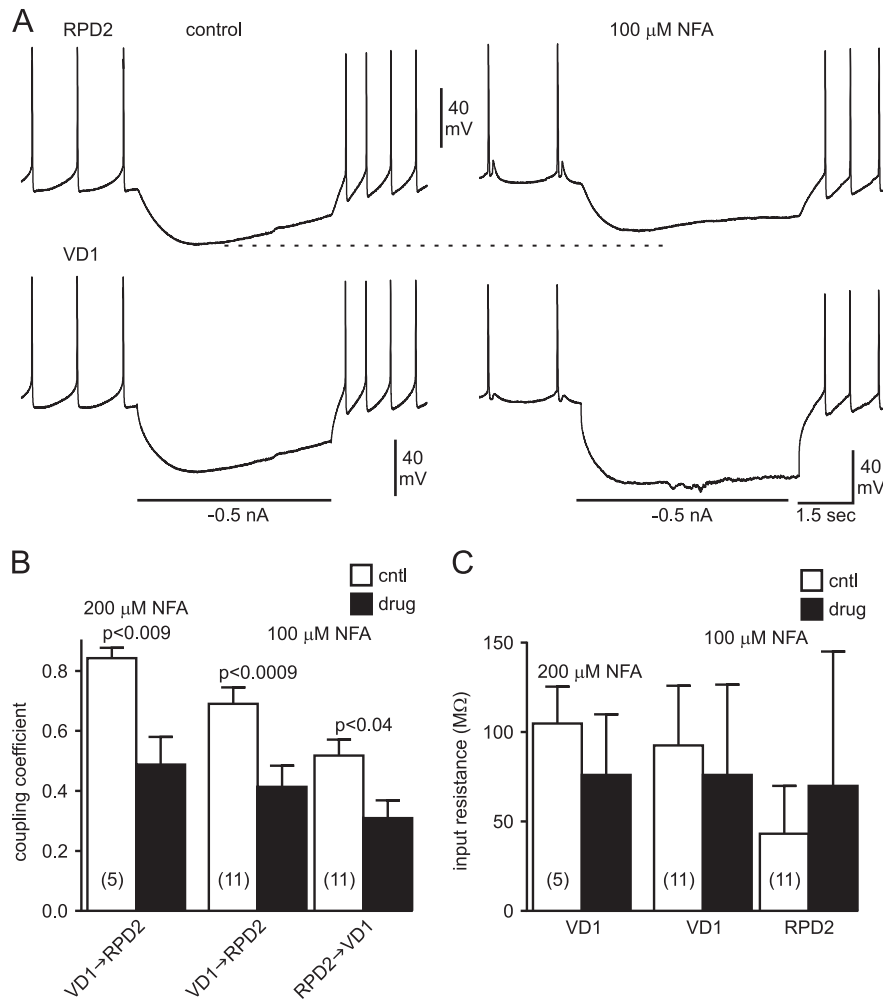


Fig. 4 – NFA attenuates $VD_1 \leftrightarrow RPD_2$ electrical coupling. (A) Coupling from VD_1 to RPD_2 assayed by injecting 0.5 nA of negative current into VD_1 before (left) and 10 min after (right) application of 100 μ M niflumic acid (NFA). NFA attenuates the $VD_1 \rightarrow RPD_2$ electrical synapse; the dotted line indicates the peak change in RPD_2 membrane potential induced by hyperpolarizing VD_1 in control. In the presence of NFA, current injection into VD_1 does not hyperpolarize RPD_2 as strongly as in control. Time base applies to all traces. (B) The $VD_1 \rightarrow RPD_2$ coupling coefficient is reduced in both 100 μ M and 200 μ M NFA, as well as the $RPD_2 \rightarrow VD_1$ coupling coefficient in 100 μ M NFA (paired Student's t-test). Number of pairs is shown within brackets where each trial represents a pair of cells before and after drug addition. (C) Input resistance, as measured from the response to 0.5 nA current injection, is not altered by NFA at 200 μ M or 100 μ M.

carbenoxolone ($n=4$), 100 μ M meclofenamic acid ($n=4$), and 300 μ M quinine ($n=6$), were ineffective (Table 2).

2.5. Gap junction blockers can cause temporary desynchronization

Although the presence of either NFA or NPPB did not appreciably alter the firing frequency or overall synchrony of the VD_1/ RPD_2 network, there were cases where modest desynchrony and changes to firing did appear following drug addition. Fig. 6 shows an example of this out-of-phase firing when 100 μ M NPPB was in the bath ($n=4$). Relative to control (Fig. 6A), where the action potentials in VD_1 and RPD_2 were completely in-phase, lowering the coupling of the network with NPPB (Fig. 6B), at times, lead to doublet spikes in VD_1 . This is likely due to reduced electric transmission delaying transfer of the spike

from VD_1 to RPD_2 , followed by inappropriate excitation of VD_1 by RPD_2 . Similar instances of desynchronization were also seen in 100 μ M NFA ($n=3$, data not shown). These occurrences of out-of-phase firing were observed in 4 out of 10 preparations for NPPB and 3 out of 11 for NFA. When these events did transpire, they initially lasted ~ 2 cycles and presented only 1–5 times during the first 5–10 min post-drug; subsequent to this time point, they became more regular and re-occurred continually. However, coupling was decreased either when desynchrony occurred or when synchrony was maintained. In NPPB, for synchronous pairs, the $VD_1 \rightarrow RPD_2$ coupling coefficient went from ~ 0.60 to ~ 0.31 , while in desynchronous pairs it went from ~ 0.73 to ~ 0.40 . For NFA, the synchronous pairs showed a change in the $VD_1 \rightarrow RPD_2$ coupling coefficient from ~ 0.75 to ~ 0.44 , while desynchronous pairs presented a shift from ~ 0.53 to ~ 0.35 . Because the extent of change in synchronous vs

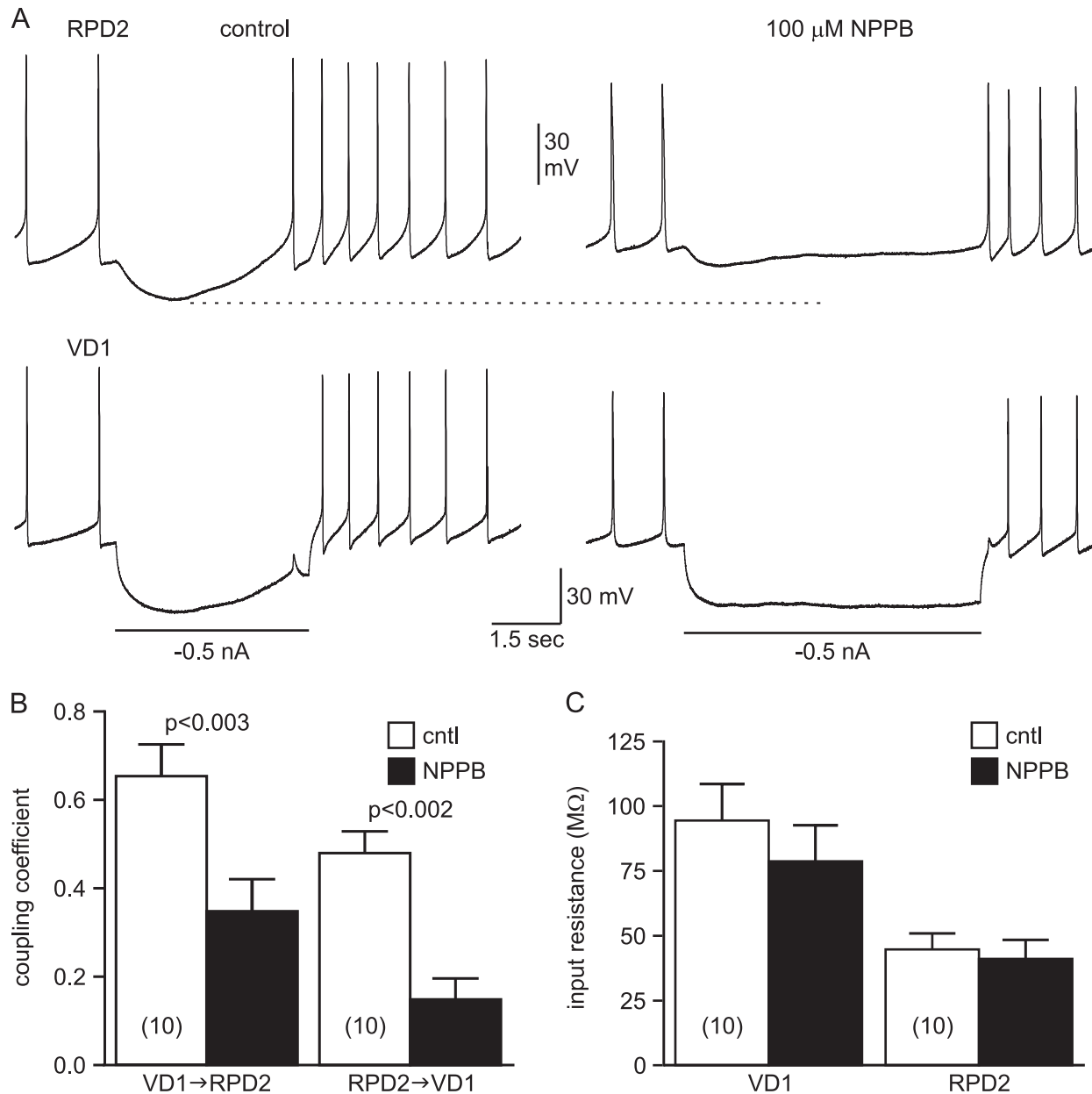


Fig. 5 – NPPB also diminishes $VD_1 \leftrightarrow RPD_2$ electrical coupling. (A) Negative current injection of 0.5 nA into VD_1 before (left) and 10 min after (right) application of 5-nitro-2-(3-phenylpropylamino) benzoic acid (NPPB) reveals a drug-induced decrease in coupling to RPD_2 . The dotted line indicates the control change in RPD_2 membrane potential before NPPB addition. In the presence of 100 μ M NPPB, hyperpolarizing VD_1 induces a weaker response in RPD_2 than in control. Time base applies to all traces. (B) Average $VD_1 \rightarrow RPD_2$ and $RPD_2 \rightarrow VD_1$ coupling coefficients are reduced by more than half following NPPB (paired Student's *t*-test). Number of pairs is shown within brackets. (C) Summary data shows input resistance of either neuron is not altered by NPPB (paired Student's *t*-test).

desynchronous pairs was similar, it suggested that the absolute effectiveness of the blockers was not the primary determinant of partial desynchronization.

2.6. Silencing VD_1 reveals decoupling in the presence of blockers

The cut commissure experiment demonstrated that VD_1 continues to fire, albeit at a somewhat reduced frequency, whereas RPD_2 discharged far more slowly and independent of

VD_1 . This was not replicated by lowering $VD_1 \leftrightarrow RPD_2$ coupling with the blockers. However, would RPD_2 still fire continuously if the drive from VD_1 was removed while also pharmacologically inhibiting the gap junction? In control preparations ($n=4$), strongly hyperpolarizing VD_1 to eliminate its drive to spike resulted in concomitant silencing of RPD_2 , due to the pronounced coupling of the network (Fig. 7A). Also, under these long periods of hyperpolarization, both VD_1 and RPD_2 exhibited oscillations in membrane potential, although neither cell fired. Yet, when a combination of 100 μ M NFA

Table 2 – Gap junction blockers that fail to inhibit the VD₁ ↔ RPD₂ electrical synapse.

Blocker	Direction	Control coupling	Drug coupling	p-Value
α-Glycyrrhetic acid (50 μM) (n=4)	VD1 → RPD2	0.65 ± 0.05	0.76 ± 0.07	> 0.05
	RPD2 → VD1	0.46 ± 0.13	0.47 ± 0.08	> 0.05
Carbenoxolone (100 μM) (n=4)	VD1 → RPD2	0.76 ± 0.07	0.62 ± 0.13	> 0.05
	RPD2 → VD1	0.59 ± 0.08	0.58 ± 0.07	> 0.05
Meclofenamic acid (100 μM) (n=4)	VD1 → RPD2	0.70 ± 0.10	0.65 ± 0.08	> 0.05
	RPD2 → VD1	0.46 ± 0.11	0.53 ± 0.06	> 0.05
Quinine (300 μM) (n=6)	VD1 → RPD2	0.65 ± 0.09	0.50 ± 0.11	> 0.05
	RPD2 → VD1	0.49 ± 0.08	0.50 ± 0.12	> 0.05

Control and drug coupling refer to the coupling coefficient before and 5 min after the addition of the indicated gap junction blocker. The p-value represents the outcome of a paired Student's t-test.

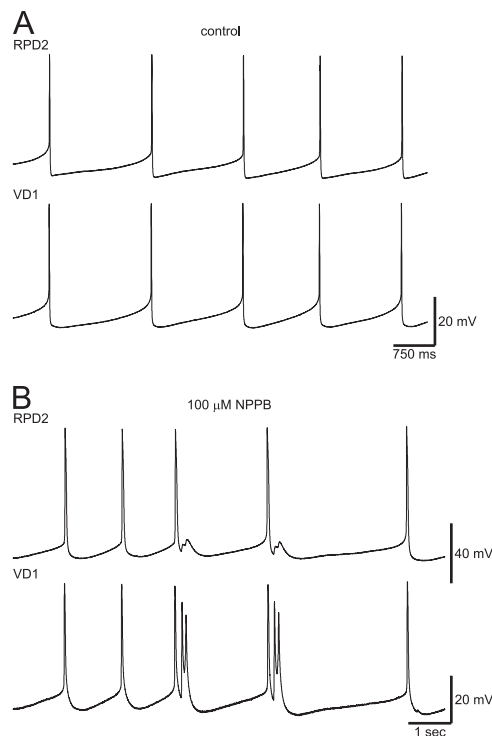


Fig. 6 – Disruption of electrical coupling with NPPB can cause temporary desynchronization. (A) Firing of VD₁ and RPD₂ under control conditions is both tonic and synchronous. Scale bars apply to both traces. (B) Approximately 6 min after addition of 100 μM NPPB, instances of desynchrony and irregular firing occur, as VD₁ is excited out of phase by a lagging action potential in RPD₂. This causes doublet spikes in VD₁, which produces electrotonic potentials in RPD₂. Time base applies to both traces.

and 100 μM NPPB was applied, to maximally inhibit the gap junctions (n=6), hyperpolarization of VD₁ failed to silence RPD₂ (Fig. 7B). Inappropriate network output was apparent, as seen by RPD₂ firing at a slower frequency (0.11 ± 0.01 Hz) and often in discrete bursts vs prior to hyperpolarization (0.68 ± 0.09 Hz). The difference in activity levels was significant ($p < 0.007$, Student's paired t-test). In addition,

electrotonic potentials could be seen in VD₁ on account of the action potentials in RPD₂.

3. Discussion

The present study examines electrical coupling within the identified VD₁/RPD₂ network and how disruption of this coupling influences synchronous output. We report that VD₁ and RPD₂ each have a distinct, but somewhat variable structure, with axons running through the confines of the CNS and different nerves. Pharmacological inhibition of the gap junction by NFA or NPPB decreases VD₁ ↔ RPD₂ coupling and occasionally causes temporary desynchronization. However, unlike the physical disruption of the gap junction through axotomy, NFA or NPPB failed to completely decouple VD₁ and RPD₂ or reveal independent firing. Furthermore, VD₁ was found to retain its firing pattern after axotomy, but in the case of gap junction inhibition, only by silencing VD₁ was *bona fide* decoupling of the network achieved. This suggests that the rhythm and frequency in the VD₁/RPD₂ network is controlled by VD₁, but requires strong electrical coupling for both neurons to synchronize.

The morphology of VD₁ and RPD₂ is largely consistent with earlier studies (e.g., Kerkhoven et al., 1991). However, using Procion yellow staining, Softe and Benjamin (1980) found that the left parietal, cutaneous pallial, and right internal parietal nerves always contained a VD₁ axon, while RPD₂ was observed to always send projections through the intestinal, anal, genital, and right internal parietal nerves. Interestingly, they also found that RPD₂ never sent axons through the left parietal, cutaneous pallial, or right external parietal nerves. These data are in contrast with our results showing axons from both neurons in 30–80% of the nerves in question, and no invariant axons. Nevertheless, our staining and that of others always shows main axons originating from both VD₁ and RPD₂, then projecting through the commissure to the contralateral ganglion. Benjamin and Pilkington (1986) provided structural and electrophysiological evidence, including intra-axonal recordings, that the VD₁ ↔ RPD₂ gap junction is located either in the visceral neuropile or the visceral-right

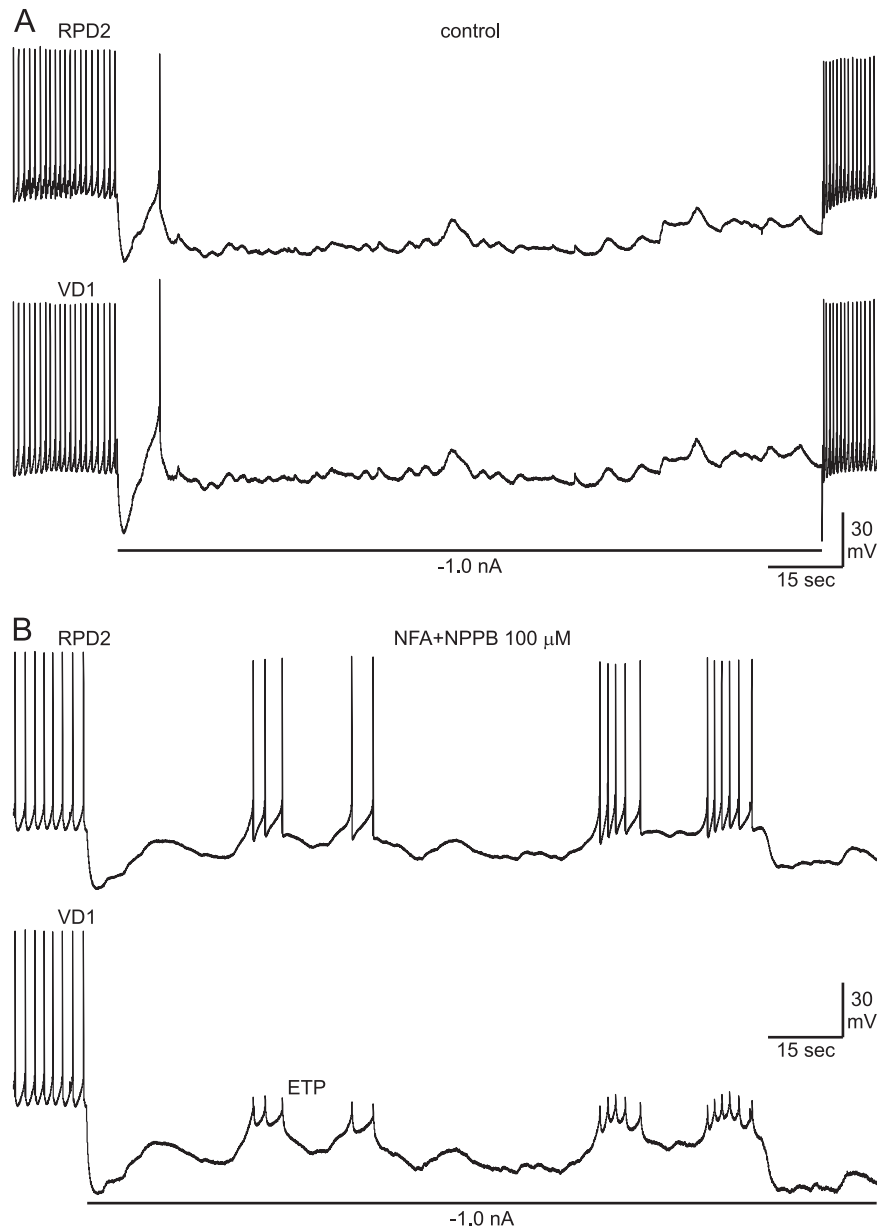


Fig. 7 – Silencing VD_1 through extended hyperpolarization reveals decoupling in the presence of NFA and NPPB. (A) Under control conditions using normal *Lymnaea* extracellular saline, prolonged (~ 2 min) current injection of negative 1 nA (at bar) into VD_1 silences both neurons. Although the cells do not reach threshold, oscillations in the membrane potential can be seen throughout the recording. Scale bars apply to both traces. **(B)** In presence of both 100 μ M NFA and 100 μ M NPPB, to block as much of the electrical synapse as possible, negative current into VD_1 fails to completely silence RPD_2 . With the gap junction attenuated, RPD_2 escapes the hyperpolarization of VD_1 and begins to fire in a slow, bursting manner. Electrotonic potentials in VD_1 are due to residual coupling. Current injection (at bar) is slowly ramped to 1 nA to keep VD_1 from firing. Scale bars apply to both traces.

parietal commissure. It was for this reason that we chose to axotomize the latter.

Discrepancies in the nature of VD_1 and RPD_2 axon projections may reflect the source of *Lymnaea*: while our animals are laboratory raised, and to a certain extent in-bred, most of the earlier work involved animals from suppliers, that were presumably wild-caught. Axonal projection variability of identified neurons has been reported previously in *Lymnaea*. Neuron Right Pedal Dorsal 1 has variant and invariant axons in visceral and right parietal nerves (Magoski and Bulloch,

1997), while Parietal A cluster neurons do not always project through the right internal parietal nerve (Wildering et al., 2001). Similarly, Left Parietal 2/3 neurons Buccal 4 neurons, present differences in peripheral nerves through which they consistently send axons (Benjamin, 1976; Benjamin et al., 1979). For other gastropods, back-filling of cerebral projections in *Aplysia*, *Archidoris*, and *Pleurobranchaea*, suggest a variability in the number cells that have axons in those nerves (Klussmann-Kolb et al., 2013). There is little consensus in the literature as to the source or mechanism of this

variability. However, if innervation patterns are indeed not the same between animals, it could represent a strategy to generate the same or similar behaviors, but using different neurons, perhaps as a means to gain efficiency or adapt to a particular selective pressure. One factor that may influence our laboratory-bred strain of *Lymnaea* is that they are reared entirely in well-aerated pond water. Potentially, such conditions preclude or result in alterations to the innervation of certain tissues, especially those associated with respiration.

There is good evidence that VD_1 is the master of the network. Through hybrid current/voltage-clamp experiments, Wildering et al. (1991a) found that transfer of the voltage command to VD_1 , i.e., making the membrane potential of VD_1 the command potential for both cells, did not introduce large changes in VD_1 or RPD_2 firing. However, transfer of the voltage command to RPD_2 dramatically slowed and made irregular the spiking activity. They also observed that when VD_1 was physically isolated and placed in short-term culture, it fired continuously at ~ 1 Hz, whereas RPD_2 fired sporadically. It appears that VD_1 has intrinsic oscillatory properties that govern the overall output of the network, and any synaptic input onto VD_1 or RPD_2 serves to modulate spiking pattern. Our data support this conclusion, given that decoupling by axotomy impacted the firing rate of RPD_2 more than VD_1 , although we did observe a less marked, but significant drop in VD_1 spiking with commissure cut, which has not been reported previously. Thus, even if VD_1 is the master, the electrical synapse appears to be important for some of the normal network output, with regenerative excitation from the spiking of RPD_2 providing some drive to VD_1 . Similar gap-junction-mediated regenerative mechanisms also provoke action potentials in motor circuits from the molluscs, *Clione* and *Tritonia* (Getting and Willows, 1974; Norekian, 1999). As for the asymmetrical $VD_1 \leftrightarrow RPD_2$ coupling, this likely arises from differences in input resistance (non-junctional conductances) between the two neurons, given that Wildering et al. (1991b) demonstrated the $VD_1 \rightarrow RPD_2$ and $RPD_2 \rightarrow VD_1$ junctional conductances to be equal under voltage-clamp.

The gap junction blockers used for the present study were largely characterized in mammalian systems, where they reduce coupling between various cells with endogenous connexins or cell lines expressing any number of connexin genes (Davidson and Baumgarten, 1988; Harks et al., 2001; Srinivas et al., 2001; Srinivas and Spray, 2003; Cruikshank et al., 2004). For invertebrates, α -glycyrrhetic acid inhibits neuronal electrical synapses in another pulmonate mollusc, *Limax* (Ermentrout et al., 2004). While in the marine gastropod, *Aplysia*, coupling among neuroendocrine bag cell neurons is reduced by NFA, NPPB, and meclofenamic acid (Dargaei et al., 2014). Thus, NFA and NPPB are effective in both *Lymnaea* and *Aplysia*, but meclofenamic acid works only in *Aplysia*, suggesting pharmacological similarities and differences in the electrical synapses of the two species.

The inability of some blockers to attenuate the $VD_1 \leftrightarrow RPD_2$ electrical synapse, as well as the species differences in blocker sensitivity, may be due to the structure of the innexins that comprise *Lymnaea* gap junction channels. For example, if the specific types of innexins vary across species, it could result in altered or absent binding sites for individual

drugs on the hemi-channels (Phelan, 2005; Sosinsky and Nicholson, 2005; Juszczak and Swiergiel, 2009). NFA and NPPB diminished the $VD_1 \leftrightarrow RPD_2$ electrical synapse in a matter of minutes, suggesting a physical block or change in gating. Given the robustness of the coupling, the density of gap junction channels may preclude complete block at any reasonable drug concentration. This may explain why application of NFA or NPPB could decrease coupling coefficient, but not eliminate synchrony. Moreover, synchronous spiking can persist even in the absence of strong coupling; for example, rat cortical or thalamic neurons, as well as *Aplysia* bag cell neurons, present fairly limited coupling in situ, yet fire action potentials in synchrony (Blankenship and Haskins, 1979; Haskins and Blankenship, 1979; Gibson et al., 1999; Traub et al., 2001; Landisman et al., 2002; Dargaei et al., 2014).

In the presence of NFA and NPPB, hyperpolarizing the master VD_1 failed to silence the follower RPD_2 . The activity seen in RPD_2 as it escapes the hyperpolarization from VD_1 most likely comes from other chemical synaptic inputs, potentially neuron Right Pedal Dorsal 11 or the Input 2 interneuron, both of which excite VD_1 and RPD_2 (Benjamin and Winlow, 1981; Syed and Winlow, 1991). Normally, the drive from VD_1 dominates the network output, and any synaptic excitation has a subtle influence on frequency. Only when coupling has been attenuated, and the drive from VD_1 removed, did we see synaptic inputs onto RPD_2 that allowed it to fire irregularly and independent of the master. When Wildering et al. (1991a) placed VD_1 and RPD_2 under hybrid current/voltage-clamp, and set the membrane potential of RPD_2 as the command voltage, similar irregular spiking was observed, and this was abolished by removal of synaptic input with low extracellular Ca^{2+} . Generally speaking, in a continuously active or bursting network, consisting of a master/follower arrangement, strong electrical coupling seems necessary for the network to maintain synchronous output and rhythm.

The output of an electrically coupled network may also be related to its physiological role (see below). Strongly coupled neurons are best suited to fire synchronously, whereas weakly coupled cells may be capable of bursting at different frequencies, with more variable patterns of activity (Selverston and Moulins, 1985). For the VD_1/ RPD_2 network, strong electrical coupling appears to be a requirement that constantly maintains a regular, synchronous output. This may provide some measure of cardio-respiratory control to keep the animal alive, particularly in light of the fact that a drop in gap junction conductance at approximately 12 months of age is correlated with a marked increase in mortality (Wildering et al., 1991b). Although age is likely not a factor in the present study, given that our *Lymnaea* were aged 2 months at the most, which is well before the onset of age-related changes in $VD_1 \leftrightarrow RPD_2$ coupling.

An unresolved question is why VD_1 and RPD_2 must fire in synchrony and what is their exact function? Many of the nerves through which the two neurons send axons innervate aspects of the cardio-respiratory system, including the heart auricle (intestinal nerve), the pneumostome (right internal and external parietal nerves), and the mantle (left parietal, cutaneous pallial, and right internal parietal nerve) (Janse, 1974). Specifically, VD_1 axons can be followed to the skin

around the pneumostome and osphradium, suggesting a role in respiration (Kerkhoven et al., 1991); moreover, both VD₁ and RPD₂ hyperpolarize upon lowering of the pO₂ in the mantle (Janse et al., 1985; Van der Wilt et al., 1987). In addition, VD₁ and RPD₂ axons can be traced to the heart, while VD₁/RPD₂ peptides are localized in heart tissue by immunohistochemistry, and some of those peptides excite the heart when applied exogenously (Kerkhoven et al., 1991; Bogerd et al., 1994; Ewadinger et al., 1996). Despite the variability in axonal projections, it is likely that at least one of VD₁ or RPD₂ would innervate the heart, mantle, and pneumostome. Thus, strong coupling and synchronous firing could assure that all of these regions receive constant peptidergic input, regardless of which cell innervates a particular region.

4. Experimental procedures

4.1. Dissection and salines

Experiments were performed using a stock of *Lymnaea stagnalis* (shell length 15–20 mm; age 1–2 months) raised and maintained in a small-scale aquaculture facility at 21–23 °C and fed Romaine lettuce and trout chow five times per week. The CNS was removed and pinned-out dorsal surface up in a Sylgard-lined 35-mm petri dish (184 Silicone Elastomer, Dow Corning, USA). The cerebral commissure was cut so that the CNS lay flat, and VD₁ and RPD₂ were exposed. Dissection, pinning-out of the CNS, and almost all electrophysiology were performed in normal *Lymnaea* saline (composed of (in mM) 51.3 NaCl, 1.7 KCl, 4.1 CaCl₂, 1.5 MgCl₂, and 5.0 N-2-hydroxyethylpiperazine-*N'*-2-ethanesulphonic acid (HEPES), adjusted to pH 7.9 with 1 M NaOH). In two sets of experiments, a high Ca²⁺/high Mg²⁺ saline was used (composition as per normal saline but with 24.6 mM CaCl₂, 1.5 mM MgCl₂, and 7.5 mM MgSO₄). Salts were obtained from Fisher Scientific (Ottawa, ON, Canada), ICN (Aurora, OH, USA), or Sigma-Aldrich (St. Louis, MO, USA).

4.2. Electrophysiology

To facilitate microelectrode penetration, the sheath surrounding the CNS was exposed to a small protease crystal (type XIV; P5147, Sigma Aldrich) followed by a rinse in cold (~4 °C) normal saline. Using the bridge-balanced, sharp-electrode current-clamp technique, VD₁ and RPD₂ were impaled with glass microelectrodes (30–50 MΩ) filled with 0.5 M KCl and the membrane potential was recorded. Microelectrodes were pulled from borosilicate glass capillaries (1.2-mm external diameter, TW120F-4; World Precision Instruments, Sarasota, FL, USA) and bridge balanced with 20-ms, 0.1–0.2-nA square, hyperpolarizing current pulses. Electrophysiological measurements were made with two single-electrode amplifiers (Neuroprobe 1600, A-M Systems, Sequim, WA, USA), where the amount of current flow across VD₁ or RPD₂ was controlled and their respective membrane potential monitored simultaneously. Current was injected into the neurons using the direct current injection function on the amplifier. Voltage was filtered at 5 kHz using the

Neuroprobe built-in Bessel filter and sampled at 2 kHz using an IBM-compatible personal computer, a Digidata 1322A analog-to-digital converter (Molecular Devices, Sunnyvale, CA, USA), and the AxoScope acquisition program (8.2; Molecular Devices). To measure coupling coefficient and input resistance, a negative current of 0.5 nA was injected for 3–5 s into either VD₁ or RPD₂, and the resultant hyperpolarization from both cells recorded.

4.3. Intracellular dye staining and fluorescence microscopy

The morphology of VD₁ and RPD₂ was examined in *Lymnaea* CNS preparations by ionophoretically injecting Lucifer yellow according to methods from Magoski and Bulloch (1997). Briefly, microelectrode tips were filled with 4% w/v Lucifer yellow CH (Molecular Probes, L-453) dissolved in 0.1% lithium chloride, and the microelectrodes were then back-filled with 0.1% lithium chloride. VD₁ and/or RPD₂ were impaled and the dye was injected with constant (0.5 nA) hyperpolarizing current for 30 min. After staining, the preparations were left overnight at 4 °C in normal saline, and then fixed for 3 h in 3.7% (v/v) formaldehyde (BDH; B28421) in phosphate buffer (132.3 mM Na₂HPO₄ and 25.2 mM NaH₂PO₄ × H₂O; pH 7.3). CNS were then dehydrated in a series of ethanol washes: 50%, 70%, 90%, and 100% ethanol (2 × 30 min), followed by defatting for 10 min in dimethyl sulfoxide (DMSO; BP231; Fisher), and then cleared and mounted in methyl salicylate (Sigma; M6752). Stained preparations were imaged with a Nikon TS100-F inverted microscope (Nikon, Mississauga, ON, Canada), equipped with a Nikon Plan Fluor 4X (numerical aperture (NA)=0.13), 10 × (NA=0.30), and 20 × (NA=0.50) objectives and a 50-W mercury lamp. Excitation was provided by a 470/20-nm band pass filter, and the fluorescence emitted to the eyepiece or camera through a 505-nm dichroic mirror and 520-nm long pass filter. Images (1392 × 1040 pixels) were acquired using a Pixelfly USB camera (Photon Technology International, London, ON, Canada) and the Micro-Manager 1.4.5 plugin (<http://micro-manager.org>) for ImageJ 1.44n9 (<http://rsbweb.nih.gov/ij/>) with 500–3000 ms exposure times.

4.4. Drug application and reagents

Drugs were applied as a small volume (<10 μl) of concentrated stock solution mixed with a larger volume of saline (~100 μl) that was initially removed from the bath then pipetted back. Care was taken to add drugs near the side of the dish and as far away as possible from the CNS. Measurements of coupling coefficient were taken after 5 min of exposure to a given reagent. Gap junction blockers were all dissolved in DMSO as stock solutions: niflumic acid (100 mM stock, 100 or 200 μM final; N0630, Sigma-Aldrich), meclofenamic acid (50 mM stock, 100 μM final; M4531, Sigma-Aldrich), 5-nitro-2-(3-phenylpropylamino) benzoic acid (50 mM stock, 100 μM final; N4779, Sigma-Aldrich), quinine (100 mM stock, 300 μM final; Q-1250, Sigma-Aldrich), α-glycyrrhetic acid (100 mM stock, 50 μM final; G8503, Sigma-Aldrich), and carbenoxolone (50 mM stock, 100 μM final; C4790, Sigma-Aldrich).

4.5. Data analysis

The coupling coefficient was calculated at each time point (before blocker addition and after) with the following: ΔV_m neuron 2/ ΔV_m neuron 1, where neuron 1 was the cell injected with hyperpolarizing current, neuron 2 was the cell to which neuron 1 was coupled, and ΔV_m was the change in membrane potential once hyperpolarized. The Clampfit analysis program of pCLAMP (10.2) was used to determine the ΔV_m of both cells after hyperpolarizing current injection. Cursors were placed at the baseline voltage, before injection, as well as the peak voltage drop after the injection. The difference between the two cursor values was taken as the ΔV_m . The input resistance was also calculated before and after drug addition with the following: ΔV_m neuron 1/current injected. The negative current injected into cells was 0.5 nA. The ΔV_m was taken from baseline membrane potential to the peak reached during either the steady-state or the sag of the hyperpolarization. The Clampfit analysis program was also used to determine the firing frequency of neurons, where baseline and threshold markers were set relative to the resting membrane potential of one or both cells to quantify the number of action potentials over time. Typically, we counted spikes for 5–10 min of a recording during control and, if applicable, a similar amount of time following drug. Finally, firing synchrony was measured by comparing the time-shifted data between VD₁ and RPD₂ pairs over periods of 5–10 min using the cross-correlation analysis function in Clampfit with the number of lags at ± 1000 .

Coupling coefficient and input resistance data of the VD₁/RPD₂ system are presented as means \pm standard error of the mean. Statistical analysis was performed using InStat (version 3; GraphPad Software, San Diego, CA). The Kolmogorov–Smirnov method was used to test data sets for normality. Student's paired or unpaired *t*-test was used to test whether the mean differed between two groups, while an ordinary one-way analysis of variance (ANOVA) with the Dunnett multiple comparisons test was used to test for differences between multiple means. The level of significance of the two-tailed *p* value was set at <0.05 .

Acknowledgments

This work was supported by a Discovery grant from the Natural Sciences and Engineering Research Council of Canada (#RGPIN 386664). The authors thank Heather Hodgson, Zahra Dargaei, Chris Groten and Raymond Sturgeon for technical assistance and advice.

REFERENCES

- Apostolides, P.F., Trussell, L.O., 2014. Control of interneuron firing by subthreshold synaptic potentials in principal cells of the dorsal cochlear nucleus. *Neuron* 83, 324–330.
- Benjamin, P.R., 1976. Interganglionic variation in cell body location of snail neurones does not affect synaptic connections or central axonal projections. *Nature* 260, 338–340.
- Benjamin, P.R., Rose, R.M., Slade, C.T., Lacy, M.G., 1979. Morphology of identified neurones in the buccal ganglia of *Lymnaea stagnalis*. *J. Exp. Biol.* 80, 119–135.
- Benjamin, P.R., Winlow, W., 1981. The distribution of three wide-acting synaptic inputs to identified neurons in the isolated brain of *Lymnaea stagnalis* (L.). *Comp. Biochem. Physiol.* 70A, 293–307.
- Benjamin, P.R., Pilkington, J.B., 1986. The electrotonic location of low-resistance intercellular junctions between a pair of giant neurones in the snail *Lymnaea*. *J. Physiol.* 370, 111–126.
- Bennett, M.V.L., 2000. Seeing is relieving: electrical synapses between visualized neurons. *Nat. Neurosci.* 3, 7–9.
- Bennett, M.V.L., Zukin, R.S., 2004. Electrical coupling and neuronal synchronization in the mammalian brain. *Neuron* 41, 495–511.
- Berry, M.S., Pentreath, V.W., 1976. Criteria for distinguishing between monosynaptic and polysynaptic transmission. *Brain Res.* 105, 1–20.
- Blankenship, J.E., Haskins, J.T., 1979. Electrotonic coupling among neuroendocrine cells in *Aplysia*. *J. Neurophysiol.* 42, 347–355.
- Bogerd, J., Geraerts, W.P., Van, H.H., Kerkhoven, R.M., Joosse, J., 1991. Characterization and evolutionary aspects of a transcript encoding a neuropeptide precursor of *Lymnaea* neurons, VD1 and RPD2. *Brain Res. Mol. Brain Res.* 11, 47–54.
- Bogerd, J., Li, K.W., Jiménez, C.R., van der Schors, R.C., Ebberink, R.H., Geraerts, W.P., 1994. Processing, axonal transport and cardioregulatory functions of peptides derived from two related prohormones generated by alternative splicing of a single gene in identified neurons VD1 and RPD2 of *Lymnaea*. *Brain Res. Mol. Brain Res.* 23, 66–72.
- Cao, G., Nitabach, M.N., 2008. Circadian control of membrane excitability in *Drosophila melanogaster* lateralventral clock neurons. *J. Neurosci.* 28, 6493–6501.
- Cruikshank, S.J., Hopperstad, M., Younger, M., Connors, B.W., Spray, D.C., Srinivas, M., 2004. Potent block of Cx36 and Cx50 gap junction channels by mefloquine. *Proc. Natl. Acad. Sci. USA* 101, 12364–12369.
- Dargaei, Z., Colmers, P.L.W., Hodgson, H.M., Magoski, N.S., 2014. Electrical coupling between *Aplysia* bag cell neurons: characterization and role in synchronous firing. *J. Neurophysiol.* 112, 2680–2696.
- Davidson, J.S., Baumgarten, I.M., 1988. Glycyrhethinic acid derivatives: a novel class of inhibitors of gap-junctional intercellular communication. Structure–activity relationships. *J. Pharmacol. Exp. Ther.* 246, 1104–1107.
- Diamond, J., Huxley, A.F., 1968. The activation and distribution of GABA and L-glutamate receptors on goldfish Mauthner neurones: an analysis of dendritic remote inhibition. *J. Physiol.* 194, 669–723.
- Ermentrout, G.B., 1985. The behavior of rings of coupled oscillators. *J. Math. Biol.* 23, 55–74.
- Ermentrout, B., Wang, J., Flores, J., Gelperin, A., 2004. Model for transition from waves to synchrony in the olfactory lobe of *Limax*. *J. Comput. Neurosci.* 17, 365–383.
- Ewadinger, N.M., Syed, N.I., Lukowiak, K., Bulloch, A.G.M., 1994. Differential tracer coupling between pairs of identified neurones of the mollusc, *Lymnaea stagnalis*. *J. Exp. Biol.* 192, 291–297.
- Ewadinger, N.M., Ridgway, R.L., Syed, N.I., Lukowiak, K., Bulloch, A.G.M., 1996. Identification and localization of a [Met⁵]-enkephalin-like peptide in the mollusk, *Lymnaea stagnalis*. *Brain Res.* 737, 1–15.
- Furshpan, E., Potter, D., 1959. Transmission at the giant motor synapses of the crayfish. *J. Physiol.* 145, 289–325.
- Gähwiler, B.H., Sandoz, P., Dreifuss, J.J., 1978. Neurones with synchronous bursting discharges in organ cultures of the hypothalamic supraoptic nucleus area. *Brain Res.* 151, 245–253.

- Galarreta, M., Hestrin, S., 1999. A network of fast-spiking cells in the neocortex connected by electrical synapses. *Nature* 402, 72–75.
- Getting, P.A., Willows, A.O., 1974. Modification of neuron properties by electrotonic synapses. II. Burst formation by electrotonic synapses. *J. Neurophysiol.* 37, 858–868.
- Getting, P.A., 1989. Emerging principles governing the operation of neural networks. *Annu. Rev. Neurosci.* 12, 185–204.
- Gibson, J.R., Beierlein, M., Connors, B.W., 1999. Two networks of electrically coupled inhibitory neurons in neocortex. *Nature* 402, 75–79.
- Harks, E.G., de Roos, A.D., Peters, P.H., de Haan, L.H., Brouwer, A., Ypey, D.L., van Zoelen, E.J., Theuvsenet, A.P., 2001. Fenamates: a novel class of reversible gap junction blockers. *J. Pharm. Exp. Ther.* 298, 1033–1041.
- Haskins, J.T., Blankenship, J.E., 1979. Interactions between bilateral clusters of neuroendocrine cells in Aplysia. *J. Neurophysiol.* 42, 356–367.
- Horn, K.G., Memelli, H., Solomon, I.C., 2012. Emergent central pattern generator behavior in gap-junction-coupled Hodgkin-Huxley style neuron model. *Comput. Intell. Neurosci.* 2012, 73910.
- Janse, C., 1974. A neurophysiological study of the peripheral tactile system of the pond snail *Lymnaea stagnalis*. *Neth. J. Zool.* 24, 93–161.
- Janse, C., van der Wilt, G.J., van der Plas, J., van der Roest, M., 1985. Central and peripheral neurones involved in oxygen perception in the pulmonate snail *Lymnaea stagnalis* (Mollusca, Gastropoda). *Comp. Biochem. Physiol.* 82A, 459–469.
- Jow, F., Numann, R., 1998. Divalent ion block of inward rectifier current in human capillary endothelial cells and effects on resting membrane potential. *J. Physiol.* 512, 119–128.
- Juszczak, G.R., Swiergiel, A.H., 2009. Properties of gap junction blockers and their behavioural, cognitive and electrophysiological effects: animal and human studies. *Prog. Neuropsychopharmacol. Biol. Psychiatry* 33, 181–198.
- Kepler, T.B., Marder, E., Abbott, L.F., 1990. The effect of electrical coupling on the frequency of model neuronal oscillators. *Science* 248, 83–85.
- Kerkhoven, R.M., Croll, R.P., Van, M.J., Bogerd, J., Ramkema, M.D., Lodder, H., Boer, H.H., 1991. Axonal mapping of the giant peptidergic neurons VD1 and RPD2 located in the CNS of the pond snail *Lymnaea stagnalis*, with particular reference to the innervation of the auricle of the heart. *Brain Res.* 565, 8–16.
- Kerkhoven, R.M., Croll, R.P., Ramkema, M.D., Van Minnen, J., Bogerd, J., Boer, H.H., 1992. The VD1/RPD2 neuronal system in the central nervous system of the pond snail *Lymnaea stagnalis* studied by in situ hybridization and immunocytochemistry. *Cell Tissue Res.* 267, 551–559.
- Klusmann-Kolb, A., Croll, R.P., Staubach, S., 2013. Use of axonal projection patterns for the homologisation of cerebral nerves in Opisthobranchia, (mollusca, Gastropoda). *Front. Zool.* 10, 20.
- Landisman, C.E., Long, M.A., Beierlein, M., Deans, M.R., Paul, D.L., Connors, B.W., 2002. Electrical synapses in the thalamic reticular nucleus. *J. Neurosci.* 22, 1002–1009.
- Long, M.A., Jutras, M.J., Connors, B.W., Burwell, R.D., 2005. Electrical synapses coordinate activity in the suprachiasmatic nucleus. *Nat. Neurosci.* 8, 61–66.
- Magoski, N.S., Bulloch, A.G.M., 1997. Localization, physiology, and modulation of a molluscan dopaminergic synapse. *J. Neurobiol.* 33, 247–264.
- Norekian, T.P., 1999. GABAergic excitatory synapses and electrical coupling sustain prolonged discharges in the prey capture neural network of *Clione limacina*. *J. Neurosci.* 19, 1863–1875.
- Phelan, P., 2005. Innexins: members of an evolutionarily conserved family of gap-junction proteins. *Biochim. Biophys. Acta* 1711, 225–245.
- Selverston, A.I., Moulins, M., 1985. Oscillatory neural networks. *Annu. Rev. Physiol.* 47, 29–48.
- Soffe, S.R., Benjamin, P.R., 1980. Morphology of two electrotonically-coupled giant neurosecretory neurons in the snail, *Lymnaea stagnalis*. *Comp. Biochem. Physiol. A* 67, 35–46.
- Söhl, G., Maxeiner, S., Willecke, K., 2005. Expression and functions of neuronal gap junctions. *Nat. Rev. Neurosci.* 6, 191–200.
- Sosinsky, G.E., Nicholson, B.J., 2005. Structural organization of gap junction channels. *Biochim. Biophys. Acta* 1711, 99–125.
- Srinivas, M., Hopperstad, M.G., Spray, D.C., 2001. Quinine blocks specific gap junction channel subtypes. *Proc. Natl. Acad. Sci. USA* 98, 10942–10947.
- Srinivas, M., Spray, D.C., 2003. Closure of gap junction channels by arylaminobenzoates. *Mol. Pharmacol.* 63, 1389–1397.
- Syed, N.I., Winlow, W., 1991. Coordination of locomotor and cardiorespiratory networks of *Lymnaea stagnalis* by a pair of identified interneurons. *J. Exp. Biol.* 158, 37–62.
- Traub, R.D., Kopell, N., Bibbig, A., Buhl, E.H., LeBeau, F.E., Whittington, M.A., 2001. Gap junctions between interneuron dendrites can enhance synchrony of gamma oscillations in distributed networks. *J. Neurosci.* 21, 9478–9486.
- Van der Wilt, G.J., Roest, M., Janse, C., 1987. Neuronal substrates of respiratory behaviour and related functions in *Lymnaea stagnalis*. In: Boer, H.H., Geraerts, W.P.M., Joosse, J. (Eds.), *Neurobiology, Molluscan Models. Proceedings of the Second Symposium on Molluscan Neurobiology*. North Holland, Amsterdam, pp. 292–296.
- Wildering, W.C., Janse, C., de Vlieger, T.A., 1991a. The role of pacemaker properties and synaptic input in generation and modulation of spiking activity in a pair of electrically coupled peptidergic neurons. *Brain Res.* 556, 324–328.
- Wildering, W.C., van der Roest, M., de Vlieger, T.A., Janse, C., 1991b. Age-related changes in junctional and non-junctional conductances in two electrically coupled peptidergic neurons of the mollusc *Lymnaea stagnalis*. *Brain Res.* 547, 89–98.
- Wildering, W.C., Janse, C., 1992. Serotonergic modulation of junctional conductance in an identified pair of neurons in the mollusc *Lymnaea stagnalis*. *Brain Res.* 595, 343–352.
- Wildering, W.C., Hermann, P.M., Bulloch, A.G., 2001. *Lymnaea* epidermal growth factor promotes axonal regeneration in CNS organ culture. *J. Neurosci.* 21, 9345–9354.
- Yamashita, N., T Ishii, T., Ogata, E., Matsumoto, T., 1994. Inhibition of inwardly rectifying K⁺ current by external Ca²⁺ ions in freshly isolated rabbit osteoclasts. *J. Physiol.* 480, 217–224.
- Ypey, D.L., VanMeerwijk, W.P., Ince, C., Groos, G., 1980. Mutual entrainment of two pacemaker cells: a study with an electronic parallel conductance model. *J. Theor. Biol.* 86, 731.